Longitudinal patient stratification of electronic health records with flexible adjustment for clinical outcomes

Oliver Carr* OLIVER.CARR@SENSYNEHEALTH.COM
Avelino Javer* AVELINO.JAVER@SENSYNEHEALTH.COM
Patrick Rockenschaub* PATRICK.ROCKENSCHAUB@SENSYNEHEALTH.COM
Owen Parsons OWEN.PARSONS@SENSYNEHEALTH.COM
Robert Dürichen ROBERT.DURICHEN@SENSYNEHEALTH.COM
Sensyne Health Plc, Oxford, UK

Abstract

The increase in availability of longitudinal electronic health record (EHR) data is leading to improved understanding of diseases and discovery of novel phenotypes. The majority of clustering algorithms focus only on patient trajectories, yet patients with similar trajectories may have different outcomes. Finding subgroups of patients with different trajectories and outcomes can guide future drug development and improve recruitment to clinical trials. We develop a recurrent neural network autoencoder to cluster EHR data using reconstruction, outcome, and clustering losses which can be weighted to find different types of patient clusters. We show our model is able to discover known clusters from both data biases and outcome differences, outperforming baseline models. We demonstrate the model performance on 29,229 diabetes patients, showing it finds clusters of patients with both different trajectories and different outcomes which can be utilized to aid clinical decision making.

Keywords: Patient Stratification, Recurrent Neural Network, Autoencoder, Electronic Health Records, Clustering

1. Introduction

Chronic diseases like diabetes or heart failure may progress very differently across patients (Spratt et al., 2017; Lewis et al., 2017) but the reasons for differential progression are not yet well understood. Between patient differences have been linked — among other factors — to the underlying pathology or to differential response to treatment (Sarría-Santamera et al., 2020; Hedman et al., 2020).

Over the last decade, the spread of EHRs has enabled the collection of unprecedented longitudinal patient information (Shickel et al., 2018). Early work using this rich data to investigate heterogeneous disease progression mostly employed *unsupervised clustering* to find patient subgroups in the data that share a similar medical history (Miotto et al., 2016; Baytas et al., 2017; Madiraju et al., 2018; Landi et al., 2020). However, EHR data are primarily designed for clinical care and are not usually collected with research in mind. Identified clusters may therefore be driven by spurious associations such as patient drop out, selective recording, modifications of the IT infrastructure, or administrative differences between healthcare providers (de Jong et al., 2019; Ehrenstein et al., 2019).

In an attempt to address these issues, new methods have been developed that focus on relevant patient outcomes to guide the clustering of patient trajectories (Zhang et al., 2019; Lee and van der Schaar, 2020; Lee et al., 2020), e.g., by including occurrence of complications or time to death. In this so-called *predictive clustering*, a low-dimensional latent representation of the data is created that retains only information predictive of future clinical events. Patients are grouped according to their similarity in this latent space. While this approach ensures clusters that differ in the risk of experiencing the outcome, they are unable to distinguish between distinct trajectories that lead to similar risks.

Retaining trajectories, however, can be paramount to clinical interpretation. For example, although patients with acute heart failure may have short-term mortality risks that are very similar to patients hospitalised with sepsis, the mechanisms that cause the high risk are quite different and a model should be

* These authors contributed equally

able to distinguish between them. In this work, we therefore propose a novel semi-supervised architecture that combines both approaches — predictive and unsupervised — to guide clustering towards outcomes of interest while enforcing similarity on the input scale. By doing so, we ensure that patients with very different trajectories are not lumped into a common cluster but remain in separate groups that facilitate clinical interpretation. Changing the weights of the unsupervised and predictive optimisation functions, the algorithm can be adjusted to prioritise one or the other. We refer to this approach as longitudinal patient stratification by clinical outcomes (LPS-CO).

We apply our method to right-censored clinical data — which is ubiquitous in EHR data — and show how it can lead to novel insights. Our main contributions can be summarised as follows:

- Introduction of a flexible semi-supervised patient stratification approach which identifies clusters of patients which share a similar medical history as well as clinical outcomes through parallel optimisation of an unsupervised and predictive loss function.
- Introduction of a Cox proportional hazards loss function to consider right-censored outcomes as predictive targets such as time to death or rehospitalisation.

We validate our proposed method on a synthetic dataset with known clusters as well as on a diabetes cohort extracted from a longitudinal EHR dataset consisting of approximately half a million patients. Comparisons to other baseline methods indicate how our approach can balance between unsupervised and predictive clustering and discover novel patient clusters.

2. Related Work

Initial work in patient phenotyping mostly applied clustering to cross-sectional data. Patient phenotyping using k-means has been used early for example in diabetes (Hammer et al., 2003) and heart failure (Ather et al., 2009). Other commonly applied methods include hierarchical clustering (Moore et al., 2010; Burgel et al., 2010) and self-organising maps (Ather et al., 2009). Recently, these have been partially superseded by methods based on autoencoders, which provide an elegant way to deal with increasingly high-dimensional medical data. Notably, Xie et al. (2016) proposed a deep embedded clustering (DEC) algorithm that uses an autoencoder with a self-supervised loss function to jointly learn the low-dimensional representation and cluster assignments. This approach has been used in Carr et al. (2020) and Castela Forte et al. (2021), among others, and provides the basis for our proposed approach.

With the advent of EHRs and increasing availability of longitudinal patient data, unsupervised methods have also been used for phenotyping of sequential medical data. Proposed models include generalisations of classical methods (see for example Mullin et al. (2021)) as well as deep learning-based algorithms to longitudinal data. In the latter case, recurrent autoencoders (Zhang et al., 2018; de Jong et al., 2019) or convolutions (Zhu et al., 2016) have been used to embed the time series.

When evaluating the groups identified during clustering via the above methods, patients are often compared based on the risk of experiencing clinically relevant outcomes. For example, Castela Forte et al. (2021) show that among intensive care patients, cluster membership was associated with risk of death. The analysis is entirely post-hoc, however, and differences in risk did not directly influence the earlier cluster assignments. Recent works have aimed to incorporate information of outcomes into the discovery of clusters. Zhang et al. (2019) used a recurrent neural network (RNN) to predict markers of progression in Parkinson's disease and then employed dynamic time warping (Berndt and Clifford, 1994) and t-distributed Stochastic Neighbor Embedding (t-SNE) (van der Maaten and Hinton, 2008) to cluster patients based on the hidden states of the RNN. Lee and van der Schaar (2020) proposed an actor-critic approach for temporal predictive clustering (AC-TPC) in which an RNN-based encoder/predictor network is trained jointly with the cluster embeddings. This was extended in Lee et al. (2020) to incorporate time-to-event outcomes via a novel loss function based on a Weibull-shaped parametric hazard.

In our work, we have adapted a RNN autoencoder through the addition of a clustering loss (Xie et al., 2016) and an outcome loss (Bello et al., 2019) and propose flexible balancing of these losses, thereby allowing researchers to control the degree to which clinical outcomes should drive the clustering. This differs from Zhang et al. (2019); Lee and van der Schaar (2020); Lee et al. (2020) who focus on outcomes without retaining trajectory information in the clusters.

3. Methods

This section describes the methods and models used to obtain patient representations from patient trajectories and the clustering methods applied.

Let $\mathcal{D} = \{\mathcal{X}, \mathcal{Y}\}_{n=1}^{N}$ define the patient data, where $\mathcal{X}$ is a set of covariate vectors, $\mathcal{Y}$ is a set of clinical outcomes, and N is the total number of patients included in the data. $\mathcal{D}$ may describe each patient n's observations at a single point of time $\{\mathbf{x}^n, y^n\}$ or longitudinally over a period of time $\{\mathbf{x}_t^n, y_t^n\}_{t=1}^{T^n}$. Similarly, $\mathcal{Y}$ may contain continuous outcomes $y^n \in \mathbb{R}$, binary outcomes $y^n \in \{0, 1\}$, or time-to-event outcomes $y^n = \{s^n, c^n\}$ with $s^n \in \mathbb{R}^+$ being the patient's follow-up time and $c^n \in \{0, 1\}$ being an indicator of whether the patient experienced the outcome of interest (1) or was censored (0). Going forward and without loss of generality, we omit the time subscript t for simplicity and assume time-to-event data.

Following Xie et al. (2016), we aim to cluster $\mathcal{X}$ into K clusters, each of which is represented by a centroid vector λ_k for $k = 1, ..., K$. In order to deal with the challenges posed by high dimensionality frequently observed in EHR data, clustering is not performed in the input space but in a latent embedding space created by a learned, non-linear function $f_\theta : \mathcal{X} \to \mathcal{Z}$.

We combined three losses with corresponding weights to give the overall loss function,

$$L = w_r L_r + w_y L_y + w_c L_c, \tag{1}$$

where L_r represents a reconstruction loss, L_y an outcome loss, and L_c a clustering loss (Figure 1). w_* represents the weight for each loss. The network architecture and losses are described in detail in the following sections.

3.1. Patient Embedding

In our proposed method, we first train an autoencoder network and obtain a fixed-size latent embedding vector $\mathbf{z}^n$ for each patient n in $\mathcal{D}$ (Hinton and Salakhutdinov, 2006). In it's simplest form, the autoencoder consists of a fully-connected encoder network $f_\theta : \mathbb{R}^D \to \mathbb{R}^{D'}$ and a fully-connected decoder network $g_{\theta'} : \mathbb{R}^{D'} \to \mathbb{R}^D$, where D is the dimension of the input space and D' is the dimension of the latent space, with $D' < D$. The autoencoder is trained in an unsupervised manner to maximise the information about $\mathbf{x}$ retained in $\mathbf{z} = f_\theta(\mathbf{x})$ (Vincent et al., 2010). This is achieved by minimising a reconstruction loss $L_r(\mathbf{x}, \mathbf{x}')$, where $\mathbf{x}' = g_{\theta'}(\mathbf{z})$ is reconstructed from the latent embedding. In the case of mixed continuous and binary input, L_r can be defined as

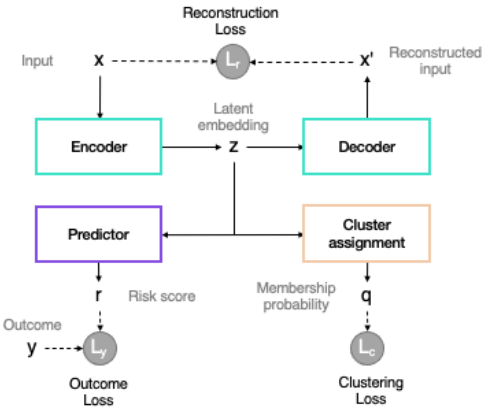

Figure 1: Schematic diagram of proposed method consisting of an autoencoder network (encoder and decoder), a predictor layer, and a cluster assignment layer.

$$L_r(\mathbf{x}, \mathbf{x}') = L_{cont} + w_b * L_{bin} \tag{2}$$

$$L_{cont} = \frac{1}{N} \sum_{n=1}^{N} (\mathbf{x}_{cont}^n - \mathbf{x'}_{cont}^n)^2 \tag{3}$$

$$L_{bin} = \frac{1}{N} \sum_{n=1}^{N} \Big\{ \mathbf{x}_{bin}^n \; log(\mathbf{x'}_{bin}^n) - (1 - \mathbf{x}_{bin}^n) \; log(1 - \mathbf{x'}_{bin}^n) \Big\} \tag{4}$$

where Equation 3 is the mean squared error of all continuous inputs $\mathbf{x}_{cont}$, Equation 4 is the binary cross entropy of all binary inputs $\mathbf{x}_{bin}$, and w_b is a weight to balance the relative contributions of each loss.

3.1.1. Alternative autoencoders

The above autoencoder can be extended to sequential patient data $\mathcal{X}_t$ by replacing the fully-connected encoder and decoder networks with a RNN. The term RNN may in this case represent any recurrent network architecture such as long short-term memory (Hochreiter and Schmidhuber, 1997) or gated recurrent unit (GRU) (Cho et al., 2014). The RNN receives time windows $\mathbf{x}_t^n$ and transforms them into a single fixed-sized embedding vector $\mathbf{z}^n$ per patient.

Additionally, the simple autoencoder described earlier may be replaced by any number of alternative architectures. For example, we found it beneficial in our experiments to use a variational autoencoder (VAE) instead (Kingma and Welling, 2014). In this case, the network learns a probabilistic rather than deterministic patient embedding (commonly parameterised as the means μ and variances σ^2 of a D' dimensional multivariate Gaussian distribution with diagonal covariance structure) which in our experiments lead to a smoother, more continuous embedding space. Using a VAE and changes L_r to

$$L_r = -\frac{1}{N}\sum_{n=1}^{N} \log p_\theta(\mathbf{x}^n|\mathbf{z}^n) - \frac{1}{2}\sum_{d'=1}^{D'}(1 + log(\sigma_{d'}^2) - \mu_{d'}^2 - \sigma_{d'}^2) \quad (5)$$

Equation 2 may be seen as a special weighted case of $\log p_\theta(\mathbf{x}|\mathbf{z})$ where all input dimensions are modelled as independently Gaussian (with fixed unit variance) or Bernoulli.

3.1.2. Pre-training of the autoencoder

As cohorts of interest often consist of much smaller numbers of patients than the total available (e.g., only patients with incident of diabetes), a pre-training step is applied to learn patient embeddings from all available data. This aims to learn a better representation between the wide range of diagnoses, procedures, medications, and laboratory measurements through time before updating the learned patient embeddings on just the cohort of interest.

3.2. Patient Outcomes

During pre-training, the autoencoder learns a lower-dimensional representation $\mathbf{z}^n$ in an unsupervised manner. We propose to include a shallow fully-connected layer h_ϕ that relates $\mathbf{z}^n$ to the risk of experiencing the outcome y^n, estimating a scalar risk score $r^n = h_\phi(\mathbf{z}^n)$.

The outcome is then included during training via the additional loss function L_y. Depending on the nature of the prediction task, L_y may be chosen as the mean squared error (regression) or binary cross-entropy (classification). For the case of right-censored time-to-event outcomes, we propose to use a loss based on the partial likelihood of the Cox proportional hazards model (Bello et al., 2019), which is defined as

$$L_y = -\frac{1}{N}\sum_{n=1}^{N} c^n \left\{ r^n - \log \sum_{j \in R(s^n)} \exp(r^j) \right\} \quad (6)$$

where c describes whether an outcome was observed for the patient ($c^n = 1$) or if the patient was censored ($c^n = 0$) and $R(s^n)$ represents the set of patients still at risk after time s^n, i.e., $R(s^n) = \{i \mid i \in \{1, ..., N\}, s^i \geq s^n\}$.

3.3. Patient Clustering

Once a patient embedding has been learned (with or without considering the outcome), standard clustering methods may be applied (see for example Zhang et al. (2019)). Alternatively, cluster assignments may be learned simultaneously with the patient embeddings, which allows them to influence the learned embeddings via back propagation and optimise them for clustering. Following Xie et al. (2016), we introduce a clustering layer that learns the position of K cluster centroids $\lambda_k \in \mathbb{R}^{D'}$. The probability q_k^n of patient embedding z^n belonging to cluster k can then be calculated via an appropriate kernel, e.g., the density of a Student's t distribution:

$$q_k^n = \frac{(1 + ||z^n - \lambda_k||^2)^{-\frac{1}{2}}}{\sum_{k'}(1 + ||z^n - \lambda_{k'}||^2)^{-\frac{1}{2}}} \quad (7)$$

Cluster assignments are then iteratively refined Xie et al. (2016). Since true cluster labels are unknown, we instead use self-training via an auxilliary target distribution p_k^n that emphasise each patient's high confidence clusters

$$p_k^n = \frac{(q_k^n)^2/f_k}{\sum_{k'}(q_{k'}^n)^2/f_{k'}} \quad (8)$$

where $f_k = \sum_{n=1}^{N} q_k^n$ is used to normalise cluster frequencies (Xie et al., 2016). By penalising large differences between q_k^n and p_k^n, the network is incentivized to pull patient embeddings towards a single (closest) centroid. The corresponding clustering loss L_c is defined as

$$L_c = \mathrm{KL}(P \parallel Q) = \frac{1}{N}\sum_{n=1}^{N}\sum_{k=1}^{K} p_k^n \log \frac{p_k^n}{q_k^n} \quad (9)$$

where $\mathrm{KL}(P \parallel Q)$ indicates the Kullback-Leibler (KL) divergence between distributions P and Q. See Xie et al. (2016) for a more detailed discussion.

3.4. Evaluation Metrics

3.4.1. Cluster Similarity

The adjusted Rand index (ARI) is used to measure the similarity between two sets of data clusters. The Rand index is defined as,

$$ARI = \frac{RI - \mathbb{E}(RI)}{max(RI) - \mathbb{E}(RI)}, \quad \text{where} \quad RI = \frac{a+b}{\binom{N}{2}}, \tag{10}$$

and $\mathbb{E}(RI)$ is the expected RI of random assignments for two sets of clusters C and K, where a represents the number of pairs of elements in the same cluster in C and K, and b represents the number of pairs of elements in different clusters in C and K.

3.4.2. KM Curves and Log Rank Test

Kaplan-Meier (KM) curves are used to evaluate the time-to-event within each of the discovered clusters (Kaplan and Meier, 1958). It measures the fraction of patients who have not experienced the event of interest by a specified time. We used log rank tests to formally compare clusters for differences in outcome risk (Harrington and Fleming, 1982). Larger values of the test statistic therefore indicate more separated curves. Note, however, that the test statistic may be driven by a large difference of only a single cluster and therefore needn't indicating separation between all clusters.

4. Data

We evaluated our model on two datasets: a synthetic EHR dataset with known clusters and a real world EHR dataset of diabetes patients from which the model is used to derive clinical insights.

4.1. Synthetic Data

We demonstrate the idealised behaviour of our proposed model within synthetic data with a known data structure. We simulated three types of clusters: unsupervised clusters, outcome clusters, and combined clusters. Unsupervised clusters, share similarities in the input space but were not associated with the outcome. These clusters are susceptible to data bias (e.g., similarities in patient trajectories due to local hospital guidance) and therefore might be of less scientific interest. Outcome clusters share the same risk of developing the event of interest but have no associated feature combinations. Combined clusters, on the other hand, represent groups of patients which share feature combinations in the input space that are associated with a higher or lower risk of developing the event of interest (e.g., a combination of factors that increase the risk of death). We hypothesise that these clusters are more clinically relevant and and their identification is the goal of this study.

The synthetic dataset is generated for $P = 60,000$ patients with the details of synthetic data generation shown in Appendix A.

4.2. Real World Data

Data was collected by the Oxford University Hospitals NHS Foundation Trust between August 2014 and March 2020 as part of routine care. The longitudinal secondary care EHR includes demographic information (i.e. sex, age), admission information (start/end dates, discharge method/destination, admission types - e.g. in-patient, outpatient, emergency department), ICD-10 coded diagnoses, OPCS-4 coded procedures, medications as British National Formulary (BNF) codes (prescribed both during visits and take-home), and laboratory measurements (e.g. blood and urine tests). Diagnosis codes could either appear in the data as a primary (indicating the primary reason for the hospital admission) or secondary diagnosis (further present comorbidities). While the majority of these are binary or categorical features, laboratory values are continuous.

Data from 493,470 patients was available for pretrain the RNN autoencoder for the initial patient trajectory embedding. Sequential data is created for all patients by grouping features in to time windows or bins. Note, even though time was not explicitly treated as a covariate, windows with no data were not removed from the sequence such that model can estimate the time difference between irregular sampled observations. Each trajectory of a patient n was divided into non overlapping time windows x_t^n of 90 days, with t being the time index. As the data spanned more than five years, this resulted in up to $t_{max} = 22$ windows per patient. Whereby features with a occurrence of $< 1\%$ were removed.

Features were extracted per time window if data was present. The binary features (primary and sec-

ondary diagnosis, procedures and medication codes) were included using multi-hot encoding. Laboratory values within a time window x_t were encoded using 6 features: *min*, *max*, *mean*, *median absolute deviation (MAD)* as well as the *last* value within the time window and *number of occurrences* per time window. The laboratory values were normalised using rank normalization (Qiu et al., 2013), where values for a given laboratory measurement were ranked according to all values in the cohort and then the ranks were normalized to the range [0, 1]. Missing binary features within a window are filled with zeros, missing continuous features are filled with -0.1, a value outside of the possible range of the normalised values. Time windows with no data were filled with an *empty* vector consisting in zeros for the binary features, and -0.1 for the continuous features. To reduce the impact of missing data points or empty time windows, these values were masked in the reconstruction loss while training the VAE.

After filtering, the total number of different features can be broken down into this feature type categories: 286 primary diagnosis codes, 351 secondary diagnosis codes, 175 procedure codes, 122 medication types and 55 laboratory values. A summary of the full cohort feature types and average lengths of trajectories are shown in Table 1.

	Diabetes Cohort	Full Cohort
# of patients	29,229	493,470
Data Windows #	272,390	2,543,106
Data Windows Avg. per Patient	9.3	5.2
Primary ICD-10 # Unique	286	286
Primary ICD-10 Avg. per Window	0.29	0.17
Primary ICD-10 Frac. of Windows	0.23	0.14
Secondary ICD-10 # Unique	351	351
Secondary ICD-10 Avg. per Window	1.9	0.8
Secondary ICD-10 Frac. of Windows	0.28	0.19
OPCS-4 # Unique	175	175
OPCS-4 Avg. per Window	0.82	0.57
OPCS-4 Frac. of Windows	0.30	0.24
Medications # Unique	122	122
Medications Avg. per Window	3.0	1.6
Medications Frac. of Windows	0.24	0.21
Lab Measurements # Unique	55	55
Lab Measurements Avg. per Window	16.1	13.9
Lab Measurements Frac. of Windows	0.89	0.85

Table 1: Statistical description of the cohorts and trajectories used. # refers to the number of patients or unique features of the different data types present. The Avg. per Window, refers to the average number of features from a given type present in a window with data. Frac. of Windows refers to the fraction of windows with data that contains at least one of the corresponding feature type.

4.2.1. Diabetes Cohort

A cohort of $29,299$ diabetes patients were selected from the full cohort to test the model on a specific cohort. Patients were included in the cohort if they had at least one primary or secondary diagnoses of diabetes, their first diagnosis of diabetes is used as an index date. Unlike the full cohort, where the trajectories are unaligned. The diabetes patient trajectories are aligned at the window containing the index event, ensuring all patients have the same number of windows (including empty windows) and the index event occurs in the same window in each patient. We investigate as a clinical outcome the risk of future cardiovascular events, of which diabetes is a risk factor. Time-to-event labels were defined as the time from index date of first diabetes diagnosis to the first occurrence of stroke, myocardial infarction, or other bleeding event. A summary of the average number of feature types and windows with data for the diabetes cohort is shown in Table 1, with a detailed feature summary in the Appendix E.

5. Results

5.1. Experiment Setup

The baseline methods include principal component analysis (PCA) with k-means clustering as an unsupervised baseline, which takes the first five principal components then applies k-means clustering.

Random survival forests (RSFs) are used as a supervised clustering baseline, to find clusters of patients who share similar time to events. A single tree of depth four is trained on 75% of features, resulting in 16 possible risk scores (one at each leaf node). This is repeated ten times with random subsets of features, resulting in each patient having ten risk scores. K-means clustering is then applied to the risk scores to obtain the final supervised clusters.

The initial RNN autoencoder model, trained on the full cohort of $493,479$ patients, was trained for 350 epochs with a batch size of $4,096$ and a learning rate of 2×10^{-3} using gradient descent with an Adam optimiser. A weight decay of 1×10^{-6} is used for regularisation, and dropout used between the GRU

layers ($p = 0.1$). The output dimension of the fully connected encoder layers was 256, with the hidden state of the GRU having dimensions of 256. The proposed LPS-CO model, trained on the diabetes cohort of 29,299 patients, was trained for 25 epochs with a batch size of 256 with the other parameters remaining the same. Hyperparamters are selected to ensure losses are converging, although no formal optimisation was applied. All models were built using PyTorch. The model architecture is described in more detail in Appendix B.

Three versions of the proposed LPS-CO model are used with different loss weights (Equation 1) for reconstruction loss, w_r, and outcome loss, w_y: no outcome loss ($w_r = 0.5$, $w_y = 0$), no reconstruction loss ($w_r = 0$, $w_y = 1$), and both reconstruction and outcome loss ($w_r = 0.05$, $w_y = 1$), these weights are chosen to ensure the losses are of similar magnitudes when combined, they have not been optimised and are left to the user depending on model requirements. In all models the KL divergence loss weight, w_{kl}, is set to 1×10^{-5} and the clustering loss weight is set to 0.25.

5.2. Synthetic Data Results

To validate the proposed model and evaluate the combination of reconstruction and outcome loss, the model was applied to the synthetic dataset. The three versions of the LPS-CO model with different loss weights were trained on the synthetic data. In addition to the proposed model, PCA k-means was trained as a baseline unsupervised clustering model, a random survival forest was trained as a baseline supervised clustering model, and an AC-TCP model proposed by Lee and van der Schaar (2020) was trained as a state-of-the-art comparison. All models were trained two times, once to find three clusters and once to find six clusters.

Table 2 shows the ARI scores comparing the discovered clusters of each models to the true labels of the unsupervised, outcome, and combined clusters of the synthetic data. PCA k-means and LPS-CO with no outcome loss were able to perfectly find the unsupervised clusters when $k = 3$ ($ARI = 1$), and could not find the outcomes clusters for $k = 3$ or combined clusters for $k = 6$ well. The random survival forest, AC-TCP, and LPS-CO with no reconstruction loss accurately found the outcomes clusters for $k = 3$. The discovered clusters for $k = 6$ shared some similarities with the true combined clusters with ARI scores of 0.50, 0.50, and 0.49 respectively.

The LPS-CO using combined reconstruction loss and outcome loss obtained the highest ARI score for the combined clusters for $k = 6$. The ARI score of 0.78 was higher than that of both the reconstruction clusters (0.02) and the outcomes clusters (0.69) indicating the model is able to ignore the large data biases in the data whilst focusing on the less prominent patterns in the input space associated with different outcomes.

	k=3			k=6		
	Unsup.	Outcome	Combined	Unsup.	Outcome	Combined
PCA k-means	1.00	0.00	0.00	0.69	0.08	0.13
RSF	0.00	0.96	0.55	0.02	0.71	0.50
AC-TCP	0.00	1.00	0.57	0.02	0.84	0.50
LPS-CO ($w_r = 0.5$, $w_y = 0$)	1.00	0.00	0.00	0.76	0.04	0.10
LPS-CO ($w_r = 0$, $w_y = 1$)	0.00	1.00	0.57	0.00	0.77	0.49
LPS-CO ($w_r = 0.05$, $w_y = 1$)	0.00	1.00	0.57	0.02	0.69	**0.78**

Table 2: Adjusted Rand index scores for baseline and proposed LPS-CO models on synthetic laboratory measure data with known unsupervised, outcome, and combined clusters.

5.3. Diabetes Dataset Results

The model is also validated on real world data with the cohort of diabetes patients and using the time to first cardiac event as the outcome. An initial patient embedding is trained on the full dataset of 493,470 patients using only the reconstruction loss before further training of the proposed clustering model on the diabetes cohort. Three versions of the model were trained on the diabetes cohort: without outcome loss, without reconstruction loss, and with combined reconstruction and outcome loss. The models were trained multiple times to find clusters from $k = 2$ to $k = 7$ resulting in 18 different scenarios. Models were trained five times on 80% of the data within each scenario and the results averaged to determine the robustness of the models.

Training without outcome loss, the models have no information about the time to cardiac event outcome, thus the clusters can only be driven by the patient trajectories up to the event of first diabetes diagnosis. Similarly, training without reconstruction loss, the models try and cluster patients who have differing outcomes and not similar trajectories. As we want to find patients who share similar trajectories and have different outcomes, ideally the model

Clusters	Recon.-Combined	Outcome-Combined	Recon.-Outcome
2	0.07 ± 0.08	0.18 ± 0.11	0.06 ± 0.09
3	0.31 ± 0.22	0.30 ± 0.23	0.13 ± 0.16
4	0.10 ± 0.02	0.21 ± 0.11	0.07 ± 0.05
5	0.15 ± 0.02	0.22 ± 0.13	0.07 ± 0.03
6	0.14 ± 0.07	0.24 ± 0.16	0.09 ± 0.05
7	0.14 ± 0.05	0.27 ± 0.07	0.07 ± 0.02

Table 3: Adjusted Rand index scores between pairs of LPS-CO clusters from different loss weights, showing similarities between the discovered clusters for each k.

with combined losses shares information with both the clusters driven by the trajectories and the clusters driven by outcomes.

Table 3 shows the mean and standard deviation of ARI scores comparing clusters found using reconstruction loss with combined loss, outcome loss with combined loss, and reconstruction loss with outcome loss. The ARI scores between the reconstruction and outcome loss clusters are low (a maximum of 0.13 ± 0.16 for $k = 3$), indicating little similarity between the discovered clusters. This is as expected due to the differing focuses on trajectories and outcomes. The ARI scores between the combined clusters and both the reconstruction and outcome clusters are higher in all cases, showing the combined loss model is learning from both trajectories and outcomes. The ARI scores between combined loss clusters and outcome loss clusters are generally higher than the scores between combined loss clusters and reconstruction loss clusters, suggesting the combined losses focus more on the outcomes.

Clusters	LPS-CO ($w_r = 0.5$, $w_y = 0$)	LPS-CO ($w_r = 0$, $w_y = 1$)	LPS-CO ($w_r = 0.05$, $w_y = 1$)
2	345 ± 171	950 ± 793	825 ± 514
3	766 ± 112	7483 ± 2691	5366 ± 2520
4	1169 ± 217	7779 ± 4773	4029 ± 4732
5	1900 ± 343	6637 ± 3846	2657 ± 884
6	1190 ± 151	5958 ± 2129	7527 ± 3036
7	1961 ± 447	10770 ± 2367	8575 ± 1955

Table 4: Log rank test statistic between reconstruction ($w_r = 0.5$, $w_y = 0$), outcome ($w_r = 0$, $w_y = 1$), and combined ($w_r = 0.05$, $w_y = 1$) loss clusters, showing separation of outcomes between the discovered clusters for each k.

Figure 2 (a) and (c) show the KM curves for the clusters found using the reconstruction loss only, combined loss, and outcome loss only models for $k = 3$. The curves estimate the time to first cardiac event for the patients in each cluster. We see that for reconstruction loss only in Figure 2 (a) the curves are less separable, with the curves for the outcome loss only in Figure 2 (c) most separable. Using combined losses in Figure 2 the separation of the KM curves are between the two other models. This is quantified in Table 4 where the mean and standard deviation of the multivariate log rank test statistic can be seen for $k = 2$ to $k = 7$ for each model. In all cases, the test statistic is highest for the outcome loss only model, indicating the highly differing KM curves, and lowest for the reconstruction loss only, indicating similar KM curves in each cluster. Again, the combined loss model is intermediate, showing it is combining both outcome and trajectory information.

Clusters	Comb. 1	Comb. 2	Comb. 3	Comb. 4	Comb. 5
Recon. 1	0.04	0.29	0.40	0.15	0.12
Recon. 2	0.01	0.13	0.42	0.10	0.34
Recon. 3	0.39	0.01	0.02	0.56	0.02
Outcome 1	0.01	0.15	0.32	0.40	0.13
Outcome 2	0.37	0.03	0.21	0.27	0.12
Outcome 3	0.00	0.43	0.07	0.10	0.40

Table 5: The fraction of patients from each cluster of the combined loss model (k=5) in each cluster of the reconstruction loss only and outcome loss only models (k=3).

We also investigate how patients in clusters found from trajectories (reconstruction loss only) and outcomes (outcome loss only) for small numbers of clusters ($k = 3$) split and are distributed through higher number of clusters ($k = 5$) using a combined loss model. Table 5 shows the distributions of patients from each of the clusters for $k = 3$ within the clusters for the combined loss model using $k = 5$.

Two cases on how clusters of patients are split going from $k = 3$ to $k = 5$ are highlighted. Patients in cluster 2 using reconstruction loss only $k = 3$, are primarily assigned to clusters 3 (42%) and 5 (54%) from the combined loss model ($k = 5$). From Figure 2 (b) we can see clusters 3 and 5 have different outcomes, yet we know the patients share similar trajectories as they are assigned to the same clusters in the reconstruction only model ($k = 3$). This indicates the combined loss model is able to find clusters of patients with similar trajectories, but different outcomes.

For the second case, patients in cluster 2 of the outcome loss only model ($k = 3$) are mainly distributed between clusters 1 (37%), 3 (21%), and 4 (27%) of the

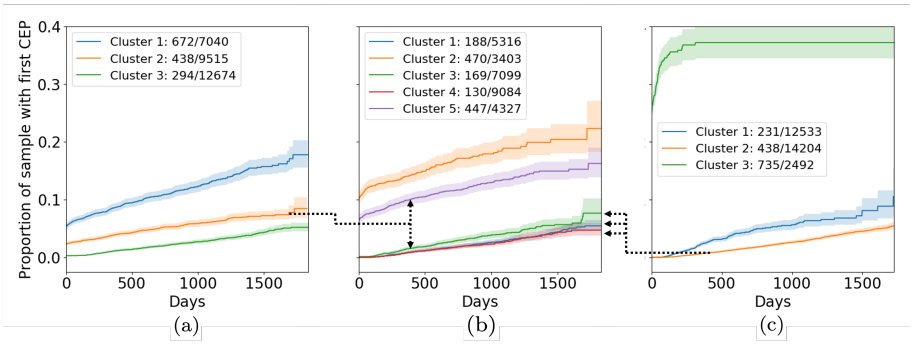

Figure 2: Kaplan-Meier curves for (a) Reconstruction loss clusters ($k = 3$, $w_r = 0.5$, $w_y = 0$), (b) combined loss clusters ($k = 5$, $w_r = 0.05$, $w_y = 1$), and (c) Outcome loss clusters ($k = 3$, $w_r = 0$, $w_y = 1$). For the values (X/Y), X shows the number of patients in the cluster who have a cardiac outcome, and Y shows the total patients in the cluster. Arrows indicate examples of how patients in clusters from the reconstruction loss and outcome loss move to new clusters in the combined loss model.

combined loss model ($k = 5$). From Figure 2 (b), we see clusters 1, 3, and 4 share similar outcomes (as in cluster 2 in Figure 2 (c)), therefore must have differing trajectories to be separate clusters. This further indicates that the combined loss model separates patients both on trajectory and outcome.

6. Discussion

We have developed a novel RNN autoencoder model to cluster patient trajectories from EHR data using a combination of losses. We combine the more standard reconstruction loss with a time-to-event loss to discover clusters of patients with both different trajectories and outcomes and evaluated it on a synthetic and real world dataset.

Our evaluation using synthetic data showed that our approach was able to find clusters based on the trajectories and outcomes (Table 2) by adjusting the weight parameters w_r and w_y of the loss functions. However, one limitation is that it is unclear how these weights should be determined when working with real EHR data with unknown underlying clusters.

Future work needs to investigate how these parameters can be optimised for a specific application. For instance, our approach can be used to identify patient cohorts which are more suited for a clinical trial (e.g. having a higher likelihood of a clinical outcome which can reduce the trial duration). In such a scenario, further criteria such as number of features to define a cluster (number of inclusion/exclusion criteria) and clinical interpretability could be included.

Another challenge is that time is not directly considered in the model. The temporal resolution of our approach was 90 days (size of a single time window). The optimal temporal granularity depends on the specific clinical question and will influence the cluster outcome. Approaches such as Baytas et al. (2017) which integrate time directly should be investigated further.

Acknowledgments

This work uses data provided by patients collected by the NHS as part of their care and support. We believe using the patient data is vital to improve health and care for everyone and would, thus, like to thank all those involved for their contribution. The data were extracted, anonymised, and supplied by the Trust in accordance with internal information governance review, NHS Trust information governance approval, and the General Data Protection Regulation (GDPR) procedures outlined under the Strategic Research Agreement (SRA) and relative Data Processing Agreements (DPAs) signed by the Trust and Sensyne Health plc.

This research has been conducted using the Oxford University Hospitals NHS Foundation Trust Clinical Data Warehouse, which is supported by the NIHR Oxford Biomedical Research Centre and Oxford University Hospitals NHS Foundation Trust. Special thanks to Kerrie Woods, Kinga Várnai, Oliver Freeman, Hizni Salih, Steve Harris and Professor Jim Davies.

References

Sameer Ather, Leif E Peterson, Vijay Divakaran, Anita Deswal, Biykem Bozkurt, and Douglas L Mann. Unsupervised cluster analysis and mortality risk in the digitalis investigation group (DIG) trial of heart failure. In *2009 International Joint Conference on Neural Networks*, pages 207–212, 2009.

Inci M. Baytas, Cao Xiao, Xi Zhang, Fei Wang, Anil K. Jain, and Jiayu Zhou. Patient Subtyping via Time-Aware LSTM Networks. In *Proceedings of the 23rd ACM SIGKDD International Conference on Knowledge Discovery and Data Mining*, pages 65–74, New York, NY, USA, 2017.

Ghalib A. Bello, Timothy J. W. Dawes, Jinming Duan, Carlo Biffi, Antonio de Marvao, Luke S. G. E. Howard, J. Simon R. Gibbs, Martin R. Wilkins, Stuart A. Cook, Daniel Rueckert, and Declan P. O'Regan. Deep-learning cardiac motion analysis for human survival prediction. *Nature Machine Intelligence*, 1(2):95–104, 2019.

D J Berndt and J Clifford. Using dynamic time warping to find patterns in time series, 1994.

P-R Burgel, J-L Paillasseur, D Caillaud, I Tillie-Leblond, P Chanez, R Escamilla, I Court-Fortune, T Perez, P Carré, N Roche, and Initiatives BPCO Scientific Committee. Clinical COPD phenotypes: a novel approach using principal component and cluster analyses. *Eur. Respir. J.*, 36(3):531–539, 2010.

Oliver Carr, Stojan Jovanovic, Luca Albergante, Fernando Andreotti, Robert Dürichen, Nadia Lipunova, Janie Baxter, Rabia Khan, and Benjamin Irving. Deep Semi-Supervised Embedded Clustering (DSEC) for Stratification of Heart Failure Patients. In *Healthcare Systems, Population Health, and the Role of Health-Tech, International Conference on Machine Learning*, 2020.

José Castela Forte, Galiya Yeshmagambetova, Maureen L. van der Grinten, Bart Hiemstra, Thomas Kaufmann, Ruben J. Eck, Frederik Keus, Anne H. Epema, Marco A. Wiering, and Iwan C.C. van der Horst. Identifying and characterizing high-risk clusters in a heterogeneous ICU population with deep embedded clustering. *Scientific Reports*, 11 (1):1–12, 2021.

Kyunghyun Cho, Bart Van Merriënboer, Caglar Gulcehre, Dzmitry Bahdanau, Fethi Bougares, Holger Schwenk, and Yoshua Bengio. Learning phrase representations using RNN encoder-decoder for statistical machine translation. *EMNLP 2014 - 2014 Conference on Empirical Methods in Natural Language Processing, Proceedings of the Conference*, pages 1724–1734, 2014.

Johann de Jong, Mohammad Asif Emon, Ping Wu, Reagon Karki, Meemansa Sood, Patrice Godard, Ashar Ahmad, Henri Vrooman, Martin Hofmann-Apitius, and Holger Fröhlich. Deep learning for clustering of multivariate clinical patient trajectories with missing values. *GigaScience*, 8(11):1–14, 2019.

V Ehrenstein, H Kharrazi, and H Lehmann. Obtaining Data From Electronic Health Records. In R E Gliklich, M B Leavy, and N A Dreyer, editors, *Tools and Technologies for Registry Interoperability, Registries for Evaluating Patient Outcomes: A User's Guide*, chapter 4. Agency for Healthcare Research and Quality (US), Rockville (MD), 3rd editio edition, 2019.

Johann Hammer, Stuart Howell, Peter Bytzer, Michael Horowitz, and Nicholas J Talley. Symptom clustering in subjects with and without diabetes mellitus: a population-based study of 15,000 australian adults. *Am. J. Gastroenterol.*, 98(2):391–398, 2003.

David P Harrington and Thomas R Fleming. A class of rank test procedures for censored survival data. *Biometrika*, 69(3):553–566, 1982.

Åsa K Hedman, Camilla Hage, Anil Sharma, Mary Julia Brosnan, Leonard Buckbinder, Li-Ming Gan, Sanjiv J Shah, Cecilia M Linde, Erwan Donal, Jean-Claude Daubert, Anders Mälarstig, Daniel Ziemek, and Lars Lund. Identification of novel pheno-groups in heart failure with preserved ejection fraction using machine learning. *Heart*, 106 (5):342–349, 2020.

G E Hinton and R R Salakhutdinov. Reducing the dimensionality of data with neural networks. *Science*, 313(5786):504–507, 2006.

Sepp Hochreiter and Jürgen Schmidhuber. Long Short-Term Memory. *Neural Computation*, 9(8): 1735–1780, 1997.

E L Kaplan and Paul Meier. Nonparametric estimation from incomplete observations. *J. Am. Stat. Assoc.*, 53(282):457–481, 1958.

Diederik P. Kingma and Max Welling. Auto-encoding variational bayes. *2nd International Conference on Learning Representations, ICLR 2014 - Conference Track Proceedings*, pages 1–14, 2014.

Isotta Landi, Benjamin S. Glicksberg, Hao Chih Lee, Sarah Cherng, Giulia Landi, Matteo Danieletto, Joel T. Dudley, Cesare Furlanello, and Riccardo Miotto. Deep representation learning of electronic health records to unlock patient stratification at scale. *npj Digital Medicine*, 3(1):1–11, 2020.

Changhee Lee and Mihaela van der Schaar. Temporal phenotyping using deep predictive clustering of disease progression. *37th International Conference on Machine Learning, ICML 2020*, pages 5723–5733, 2020.

Changhee Lee, Jem Rashbass, and Mihaela Van Der Schaar. Outcome-Oriented Deep Temporal Phenotyping of Disease Progression. *IEEE Transactions on Biomedical Engineering*, pages 1–1, 2020.

Gavin A. Lewis, Erik B. Schelbert, Simon G. Williams, Colin Cunnington, Fozia Ahmed, Theresa A. McDonagh, and Christopher A. Miller. Biological Phenotypes of Heart Failure With Preserved Ejection Fraction. *Journal of the American College of Cardiology*, 70(17):2186–2200, 2017.

Naveen Sai Madiraju, Seid M. Sadat, Dimitry Fisher, and Homa Karimabadi. Deep Temporal Clustering : Fully Unsupervised Learning of Time-Domain Features. *arXiv*, pages 1–11, 2018.

Riccardo Miotto, Li Li, Brian A Kidd, and Joel T Dudley. Deep Patient: An Unsupervised Representation to Predict the Future of Patients from the Electronic Health Records. *Scientific Reports*, 6, 2016.

Wendy C Moore, Deborah A Meyers, Sally E Wenzel, W Gerald Teague, Huashi Li, Xingnan Li, Ralph D'Agostino, Jr, Mario Castro, Douglas Curran-Everett, Anne M Fitzpatrick, Benjamin Gaston, Nizar N Jarjour, Ronald Sorkness, William J Calhoun, Kian Fan Chung, Suzy A A Comhair, Raed A Dweik, Elliot Israel, Stephen P Peters, William W Busse, Serpil C Erzurum, Eugene R Bleecker, and National Heart, Lung, and Blood Institute's Severe Asthma Research Program. Identification of asthma phenotypes using cluster analysis in the severe asthma research program. *Am. J. Respir. Crit. Care Med.*, 181(4):315–323, 2010.

Sarah Mullin, Jaroslaw Zola, Robert Lee, Jinwei Hu, Brianne MacKenzie, Arlen Brickman, Gabriel Anaya, Shyamashree Sinha, Angie Li, and Peter L Elkin. Longitudinal K-Means approaches to clustering and analyzing EHR opioid use trajectories for clinical subtypes. *J. Biomed. Inform.*, page 103889, 2021.

Xing Qiu, Hulin Wu, and Rui Hu. The impact of quantile and rank normalization procedures on the testing power of gene differential expression analysis. *BMC Bioinformatics*, 14(1):1–10, 2013.

Antonio Sarría-Santamera, Binur Orazumbekova, Tilektes Maulenkul, Abduzhappar Gaipov, and Kuralay Atageldiyeva. The identification of diabetes mellitus subtypes applying cluster analysis techniques: A systematic review. *Int. J. Environ. Res. Public Health*, 17(24), 2020.

Benjamin Shickel, Patrick James Tighe, Azra Bihorac, and Parisa Rashidi. Deep EHR: A Survey of Recent Advances in Deep Learning Techniques for Electronic Health Record (EHR) Analysis. *IEEE Journal of Biomedical and Health Informatics*, 22 (5):1589–1604, 2018.

Susan E. Spratt, Katherine Pereira, Bradi B. Granger, Bryan C. Batch, Matthew Phelan, Michael Pencina, Marie Lynn Miranda, Ebony Boulware, Joseph E. Lucas, Charlotte L. Nelson, Benjamin Neely, Benjamin A. Goldstein, Pamela Barth, Rachel L. Richesson, Isaretta L. Riley, Leonor Corsino, Eugenia R. McPeek Hinz, Shelley Rusincovitch, Jennifer Green, Anna Beth Barton, Carly Kelley, Kristen Hyland, Monica Tang, Amanda Elliott, Ewa Ruel, Alexander Clark, Melanie Mabrey, Kay Lyn Morrissey, Jyothi Rao, Beatrice Hong, Marjorie Pierre-Louis, Katherine Kelly, and Nicole Jelesoff. Assessing electronic health record phenotypes against gold-standard diagnostic criteria for diabetes mellitus. *Journal of the American Medical Informatics Association*, 24 (1):121–128, 2017.

Laurens van der Maaten and Geoffrey Hinton. Visualizing data using t-SNE. *J. Mach. Learn. Res.*, 9 (86):2579–2605, 2008.

Pascal Vincent, Hugo Larochelle, Isabelle Lajoie, Yoshua Bengio, and Pierre-Antoine Manzagol. Stacked denoising autoencoders: Learning useful representations in a deep network with a local denoising criterion. *J. Mach. Learn. Res.*, 11(110): 3371–3408, 2010.

Junyuan Xie, Ross Girshick, and Ali Farhadi. Unsupervised deep embedding for clustering analysis. *33rd International Conference on Machine Learning, ICML 2016*, 1:740–749, 2016.

Jinghe Zhang, Kamran Kowsari, James H. Harrison, Jennifer M. Lobo, and Laura E. Barnes. Patient2Vec: A Personalized Interpretable Deep Representation of the Longitudinal Electronic Health Record. *IEEE Access*, 6:65333–65346, 2018.

Xi Zhang, Jingyuan Chou, Jian Liang, Cao Xiao, Yize Zhao, Harini Sarva, Claire Henchcliffe, and Fei Wang. Data-Driven Subtyping of Parkinson's Disease Using Longitudinal Clinical Records: A Cohort Study. *Scientific Reports*, 9(1):1–12, 2019.

Zihao Zhu, Changchang Yin, Buyue Qian, Yu Cheng, Jishang Wei, and Fei Wang. Measuring patient similarities via a deep architecture with medical concept embedding. In *2016 IEEE 16th International Conference on Data Mining (ICDM)*, pages 749–758, 2016.

Appendix A. Generating Synthetic Data

When generating the synthetic clusters, we chose the variance of unsupervised clusters such that it was larger than that of combined clusters. This ensured that they were favoured by purely unsupervised clustering methods (e.g., PCA k-means or DEC), whereas semi and supervised methods (e.g., RSF, AC-TCP) are expected to find the simulated outcome clusters. However, the latter disregard different patient trajectories in the input space that lead to similar outcomes. In order to show that — depending on the weighting of the loss functions — our proposed model can also recover the specific trajectories that lead to outcomes, we further split the outcome clusters into subgroups that shared the same outcome distribution but a different covariate distribution.

The synthetic data is generated with the following steps:

- The number of noise clusters, $K_{noise} = 3$, is specified along with the number of synthetic features which contribute to these clusters, $N_{noise} = 200$. Features are sampled from isotropic Gaussian distributions with standard deviation $C_{std} = 3$ and with cluster centroids generated at random within a bounding box, $(centre_{min} = -10, centre_{max} = -10)$. The generated features are continuous and represent synthetic laboratory measures. In order to generate synthetic binary features (eg. diagnosis codes), synthetic continuous features can be passed through a min max scaler and rounded to zero or one.

- The number of outcome clusters, $K_{outcome} = 3$, is specified along with minimum and maximum time to events ($TTE_{min} = 10$, $TTE_{max} = 10,000$). The time to events are generated by sampling from exponential distributions with the scale of the distribution for each cluster one of the values log-spaced between TTE_{min} and TTE_{max} with $K_{outcome}$ steps. Censoring of events is sampled randomly from a uniform distribution ($p = 0.5$), with all time to events over a maximum threshold $(2,000)$ set to this max value and censored.

- The number of combined clusters, $K_{combined} = 6$, is set to twice the value of $K_{outcome}$ and the number of synthetic features which corre-

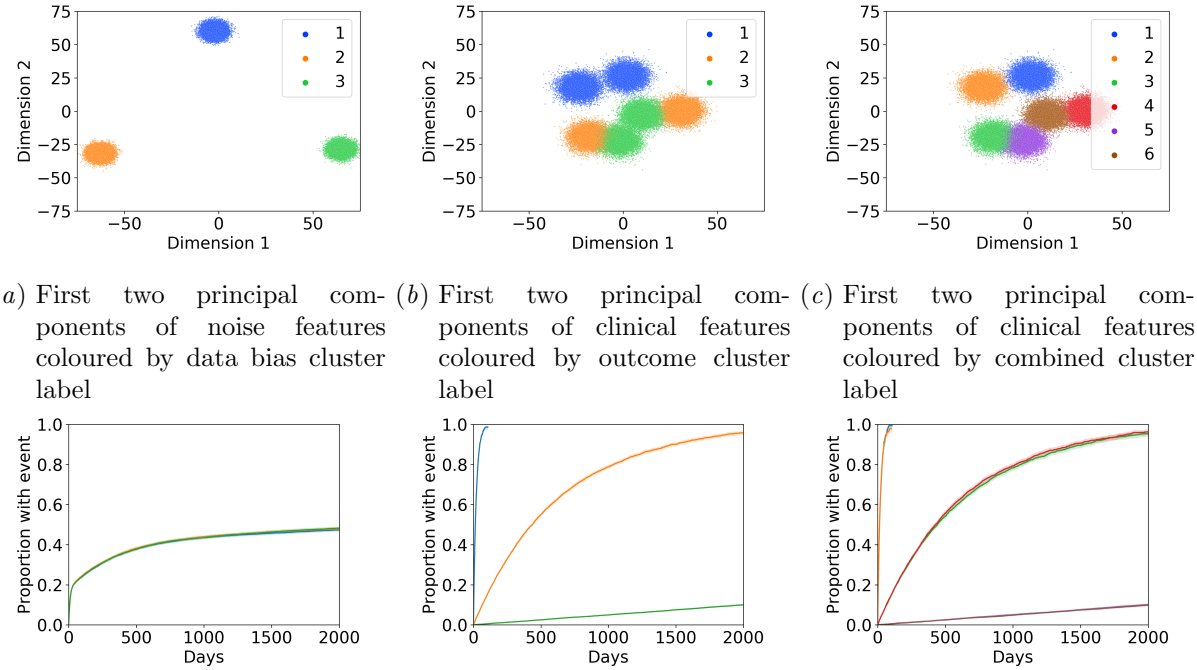

(*a*) First two principal components of noise features coloured by data bias cluster label

(*b*) First two principal components of clinical features coloured by outcome cluster label

(*c*) First two principal components of clinical features coloured by combined cluster label

(*d*) Kaplan-Meier curves of the noise clusters

(*e*) Kaplan-Meier curves of the outcome clusters

(*f*) Kaplan-Meier curves of the clinical clusters

Figure 3: Principal component plots of the data bias and combined features and the Kaplan-Meier curves of the three known cluster groups.

late with outcomes, $N_{outcome} = 200$, is specified. Each outcome cluster is randomly split in half to create the combined cluster labels. Features corresponding to the combined clusters are generated using the same method as the feature bias cluster, with smaller distances between the cluster centroids ($C_{std} = 5$, ($centre_{min} = -5, centre_{max} = -5$).

Figure 3 shows the different synthetic clusters and outcomes (as Kaplan-Meier curves). Figure 3(*a*) shows the first two principal components of PCA applied to the noise features, with the colours representing the known cluster labels. Figures 3(*b*) and 3(*c*) show the first two principal components of PCA applied to the clinical features, with the colours representing the known outcome cluster labels and clinical cluster labels respectively. Figures 3(*d*), 3(*e*), and 3(*f*) show the Kaplan-Meier curves for the outcomes of the known noise clusters, outcome clusters, and clinical clusters respectively.

Appendix B. Experiment architecture

Figure 4 shows a schematic diagram of the RNN autoencoder used to create the patient trajectory embedding in (a), using a reconstruction loss and KL divergence loss for a variational RNN autoencoder. Section (b) shows the addition clustering loss and outcome loss incorporated into the LPS-CO model to find clusters of patients who have differences in both trajectories and outcomes.

Our proposed model, a variational RNN autoencoder, is illustrated in Figure 4 (a). The encoder consists of a feature embedding layer which transforms the features of time window $\mathbf{x}_i$ into a 256 fixed-sized embedded vector using two fully connected layer with ReLU activation function. Each time window is then passed into a two layer bidirectional GRU using a dropout of 0.1 between the layers. The last hidden layer output has a dimension of 256x4 tensor (two directions times two layers). This tensor is aggregated into a 256 vector using a fully connected layer with a ReLU activation function. The aggre-

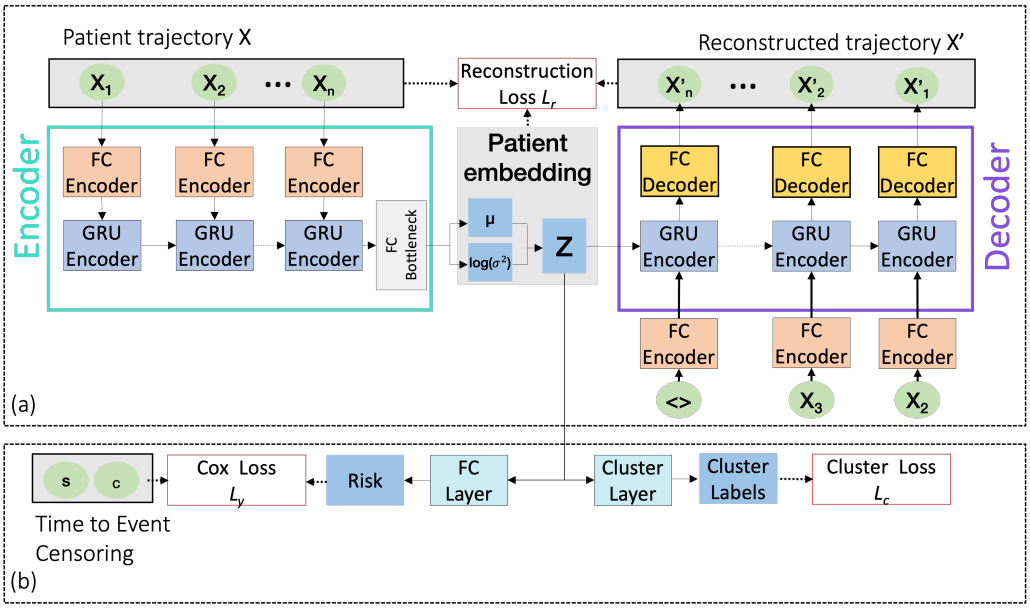

Figure 4: Schematic diagram of the RNN autoencoder. (a) shows the standard RNN autoencoder to obtain patient embeddings from trajectories. (b) shows the addition layers and loss functions to update the embedding and obtain cluster assignments.

gated vector is then feed to two separated fully connect layers producing two 256 vectors, representing the means and the log variances of the normal distributions from which the patient embedding, Z, is sampled using the re-parameterization trick Kingma and Welling (2014).

The decoder aims to predict the trajectory sequence in reverse order and uses teacher forcing during training. Therefore, the Z vector is feed as the initial hidden state of the decoder. Each time window from the input $\mathbf{x}_i + 1$ is feed into the same two layer fully connected layer and transformed into a 256 vector. Each window is then passed to a unidirectional GRU layer followed by two fully connected layers with ReLU activation that reconstruct the previous time window $\mathbf{x}'_i$.

Appendix C. Baseline Methods: Diabetes Dataset

Table 6 shows the test statistics of the log rank test between the KM curves from the clusters obtained from the baseline methods (PCA k-means and Random Survival Forests). The Kaplan-Meier curves using the baseline methods for $k = 3$ and $k = 5$ are shown in Figure 5, which correspond to the results shown in Figure 2 which use LPS-CO.

Clusters	PCA k-means	RSF
2	870 ± 3	1290 ± 52
3	1205 ± 4	1553 ± 77
4	1358 ± 2	1564 ± 67
5	1357 ± 1	1608 ± 52
6	1415 ± 5	1544 ± 35
7	1431 ± 2	1578 ± 27

Table 6: Log rank test statistic between reconstruction PCA k-means and RSF clusters, showing separation of outcomes between the discovered clusters for each k.

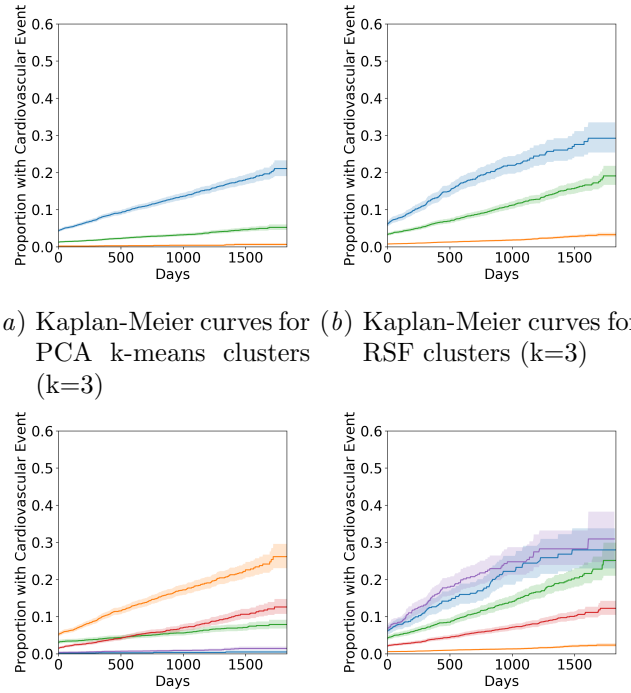

(*a*) Kaplan-Meier curves for PCA k-means clusters (k=3)

(*b*) Kaplan-Meier curves for RSF clusters (k=3)

(*c*) Kaplan-Meier curves for PCA k-means clusters (k=5)

(*d*) Kaplan-Meier curves for RSF clusters (k=5)

Figure 5: Kaplan-Meier curves for the clusters of the baseline unsupervised and supervised methods.

Appendix D. Additional Cluster Comparison Metrics

Additional clustering metrics can be used to compare the similarity of the clusters discovered using a purely unsupervised, supervised, or combined loss version of LPS-CO. Table 7 shows the normalised mutual information scores between the models for different numbers of clusters, showing the same trend as Table 3.

Clusters	Recon.-Combined	Outcome-Combined	Recon.-Outcome
2	0.05 ± 0.06	0.16 ± 0.09	0.06 ± 0.09
3	0.26 ± 0.18	0.29 ± 0.17	0.11 ± 0.13
4	0.12 ± 0.02	0.24 ± 0.09	0.08 ± 0.05
5	0.21 ± 0.03	0.26 ± 0.10	0.10 ± 0.05
6	0.18 ± 0.08	0.29 ± 0.12	0.13 ± 0.06
7	0.20 ± 0.05	0.35 ± 0.07	0.11 ± 0.02

Table 7: Normalised mutual information scores between pairs of LPS-CO clusters from different loss weights, showing similarities between the discovered clusters for each k.

Appendix E. Data Summary

Table 8 shows a summary of demographic information for the diabetes cohort, including the distributions of gender, ethnicity, and age across the 29,229 patients.

Table 9 shows the distribution (10th, 50th, 90th percentiles) of the most commonly occurring laboratory values for the diabetes cohort patients. The table is ordered by the total number of patients who have at least one measurement of the laboratory measure across their trajectory (summarised by the Counts per Patient column).

Tables 10 and 11 summarise the most occurring 20 primary and secondary diagnoses codes respectively. The tables are ordered by the total number of patients in the diabetes cohort who have at least one recorded diagnosis of the code across their trajectory. Similarly, Table 12 shows the most occurring procedure codes appearing in the diabetes cohort patients, and Table 13 shows to most occurring medication codes.

Gender		
Male	*Female*	*Unknown*
16,824	12,403	2

Ethnicity		
White British	*Not Stated*	*Other*
20,271	5,256	3,702

Age		
10th	*50th*	*90th*
46.84	69.04	84.82

Table 8: Summary of demographic information of the diabetes cohort. Counts of gender, ethnicity, and percentiles of age are shown.

Laboratory Measurement Name	Counts per Patient (Total=29,229)	Percentile 10th	50th	90th
Blood Creatinine (umol/l)	26,769	54.00	78.00	142.00
Blood Sodium (mmol/l)	26,746	134.50	138.75	141.75
Blood Potassium (mmol/l)	26,740	3.70	4.10	4.70
Blood Estimated Glomerular Filtration Rate eGFR (ml/min/1.73m2)	26,669	38.00	78.00	90.00
Blood White Blood Cells WBC (10e9/l)	26,196	5.62	8.10	11.81
Blood Haemoglobin (g/dl)	26,195	10.28	13.00	15.20
Blood Mean Corpuscular Haemoglobin Concentration MCHC (g/l)	26,193	311.00	327.00	342.00
Blood Mean Corpuscular Volume MCV (fl)	26,193	82.95	89.80	96.70
Blood Mean Corpuscular Haemoglobin MCH (pg)	26,193	26.60	29.50	31.90
Blood Red Blood Cell RBC Count (10e12/l)	26,193	3.54	4.44	5.18
Blood Haematocrit HCT (l/l)	26,193	0.32	0.40	0.46
Blood Platelets (10e9/l)	26,188	170.00	251.00	361.00
Blood Albumin (g/l)	24,998	29.00	37.00	42.00
Alkaline Phosphatase ALP (iu/l)	24,956	57.00	88.50	187.50
Blood Bilirubin (umol/l)	24,880	5.00	9.00	17.00
Alanine Aminotransferase ALT (iu/l)	24,879	12.00	21.00	45.00
Blood Urea (mmol/l)	23,702	3.75	6.00	12.80
Blood Mean Platelet Volume MPV (fl)	22,331	9.50	10.60	12.00
Blood C Reactive Protein CRP (mg/l)	20,866	1.10	10.45	100.00
Blood HDL Cholesterol (mmol/l)	18,661	0.80	1.10	1.65
Blood Total Cholesterol (mmol/l)	18,661	3.10	4.15	5.75
Blood Cholesterol HDL Ratio (ratio)	18,656	2.50	3.65	5.50
Blood Glucose (mmol/l)	16,917	5.50	8.20	14.65
Thyroid Stimulating Hormone TSH (mu/l)	16,198	0.68	1.67	3.60
Blood International Normalised Ratio INR (ratio)	15,098	1.00	1.05	2.20
Urine Creatinine (mmol/24h)	14,716	3.41	7.45	14.70
Blood Triglycerides (mmol/l)	14,096	0.84	1.57	3.14
Urine Albumin (mg/l)	13,768	0.01	0.01	0.12
Blood LDL Cholesterol (mmol/l)	13,525	1.30	2.15	3.50
Urine Albumin Creatinine Ratio (mg/mmol)	11,557	0.60	2.00	20.90
Blood B12 (pg/ml)	9,146	202.25	354.00	751.00
Blood Ferritin (ug/l)	8,906	17.80	88.91	413.23
Blood Folate (ug/l)	8,044	3.20	6.40	14.30
Blood Iron (umol/l)	7,448	5.00	11.10	19.31
Blood Transferrin (g/l)	7,448	1.81	2.58	3.36
Blood Transferrin Saturation (Blood Troponin I (ng/l)	6,126	20.00	40.00	897.25
Blood Erythrocyte Sedimentation Rate ESR (mm/h)	4,538	2.00	14.00	53.00
Blood Vitamin D VitD (nmol/l)	3,554	18.00	41.00	79.07
Blood Gamma Glutamyl Transferase GGT (iu/l)	3,427	18.00	47.25	262.25
Blood Thyroxine T4 (pmol/l)	3,278	11.08	14.10	18.90

Table 9: Values of most frequent laboratories values. The counts correspond to the number of patients that have at least one measurement along its trajectory. The percentiles presented correspond to the distribution of the median values of each patient along its trajectory.

Primary Diagnoses	Counts per Patient (Total=29,229)
H26.9 Cataract, unspecified	1,595
I25.1 Atherosclerotic heart disease	1,449
R07.4 Chest pain, unspecified	1,286
N39.0 Urinary tract infection, site not specified	712
K63.5 Polyp of colon	710
J18.9 Pneumonia, unspecified	573
N18.5 Chronic kidney disease, stage 5	558
J18.1 Lobar pneumonia, unspecified	554
D63.8 Anaemia in other chronic diseases classified elsewhere	505
D50.9 Iron deficiency anaemia, unspecified	450
J22 Unspecified acute lower respiratory infection	426
Z03.5 Observation for other suspected cardiovascular diseases	415
G47.3 Sleep apnoea	412
H25.1 Senile nuclear cataract	403
A09.9 Gastroenteritis and colitis of unspecified origin	383
H36.0 Diabetic retinopathy	382
N17.9 Acute renal failure, unspecified	367
I21.4 Acute subendocardial myocardial infarction	359
R06.0 Dyspnoea	356
C44.3 Skin of other and unspecified parts of face	347

Table 10: Counts primary diagnosis codes which occur at least once in the trajectory of patients in the diabetes cohort.

Secondary Diagnoses	Counts per Patient (Total=29,229)
E11.9 Non-insulin-dependent diabetes mellitus: Without complications	24,425
I10 Essential (primary) hypertension	17,190
Z92.2 Personal history of long-term (current) use of other medicaments	6,969
I25.9 Chronic ischaemic heart disease, unspecified	3,267
Z92.1 Personal history of long-term (current) use of anticoagulants	3,196
Z86.7 Personal history of diseases of the circulatory system	2,995
E78.0 Pure hypercholesterolaemia	2,980
I25.1 Atherosclerotic heart disease	2,951
Z86.4 Personal history of psychoactive substance abuse	2,892
J45.9 Asthma, unspecified	2,887
F17.1 Harmful use	2,881
I25.2 Old myocardial infarction	2,702
Z88.0 Personal history of allergy to penicillin	2,531
E10.9 Insulin-dependent diabetes mellitus: Without complications	2,008
I48 Atrial fibrillation and flutter	1,930
F32.9 Depressive episode, unspecified	1,915
I48.9 Atrial fibrillation and atrial flutter, unspecified	1,898
N17.9 Acute renal failure, unspecified	1,881
J44.9 Chronic obstructive pulmonary disease, unspecified	1,843
E03.9 Hypothyroidism, unspecified	1,826

Table 11: Counts secondary diagnosis codes which occur at least once in the trajectory of patients in the diabetes cohort.

Procedures	Counts per Patient (Total=29,229)
Y98.1 Radiology of one body area (or ¡ 20 minutes)	5,471
Z94.2 Right sided operation	5,083
Z94.3 Left sided operation	4,860
Y53.4 Approach to organ under fluoroscopic control	3,421
U20.1 Transthoracic echocardiography	3,335
Y97.3 Radiology with post contrast	2,917
U21.2 Computed tomography NEC	2,853
U05.1 Computed tomography of head	2,776
Z94.1 Bilateral operation	2,106
G45.1 Fibreoptic endoscopic examination of upper gastrointestinal tract	1,985
Z92.6 Abdomen NEC	1,815
Z27.4 Duodenum	1,798
O16.1 Pelvis NEC	1,788
C75.1 Insertion of prosthetic replacement for lens NEC	1,779
C87.3 Tomography evaluation of retina	1,777
C71.2 Phacoemulsification of lens	1,766
Y98.2 Radiology of two body areas	1,620
Y53.2 Approach to organ under ultrasonic control	1,555
U10.6 Myocardial perfusion scan	1,353
Z28.6 Sigmoid colon	1,068

Table 12: Counts procedure codes which occur at least once in the trajectory of patients in the diabetes cohort.

Medications	Counts per Patient (Total=29,229)
Analgesics (INP)	14,451
Anticoagulants And Protamine (INP)	12,385
Analgesics (TTA)	11,718
Antibacterial Drugs (INP)	11,686
Drugs Used In Diabetes (TTA)	11,558
Lipid-Regulating Drugs (TTA)	10,928
Drugs Used In Diabetes (INP)	10,708
Hypertension and Heart Failure (TTA)	9,938
Lipid-Regulating Drugs (INP)	8,666
Antisecretory Drugs+Mucosal Protectants (TTA)	8,563
Antisecretory Drugs+Mucosal Protectants (INP)	8,047
Hypertension and Heart Failure (INP)	7,610
Antiplatelet Drugs (TTA)	7,022
Antibacterial Drugs (TTA)	6,791
Acute Diarrhoea (INP)	6,688
Antiplatelet Drugs (INP)	6,362
Acute Diarrhoea (TTA)	6,124
Drugs Used In Nausea And Vertigo (INP)	5,999
Beta-Adrenoceptor Blocking Drugs (TTA)	5,885
Diuretics (TTA)	5,586

Table 13: Counts medication codes which occur at least once in the trajectory of patients in the diabetes cohort.